Supplementary Material

Substituent-controlled quantum interference tuning of spin and thermoelectric transport in triphenylmethyl diradical junctions

Zhenhai Cui[1], Yongfeng Xiong[2], Qiuming Liu[1], Ziqiang Liu[2], Tong Chen[2], Lin Huang[2*]

[1] *School of Software Engineering, Jiangxi University of Science and Technology, Nanchang 330013, China*

[2]*School of Energy and Mechanical Engineering, Energy materials computing center, Jiangxi University of Science and Technology, Nanchang 330013, China*

*Corresponding author (Lin Huang): lin_huang@hnu.edu.cn

1. Mulliken population analysis.

As shown in Table S1, we performed Mulliken population analysis for the R1–R4 molecular junctions to examine their charge-transfer behavior. The charge-transfer values for R1–R4 are 0.28 e, 0.29 e, 0.31 e, and 0.30 e, respectively, indicating moderate charge transfer in all systems. However, as discussed in the main text, the R1–R3 junctions retain finite spin polarization, suggesting that the transferred charge is insufficient to quench their local magnetic moments. In contrast, the R4 junction exhibits stronger charge transfer that is capable of suppressing the local magnetic moment, thereby driving the system into a closed-shell configuration.

Table S1. Charge transfer in the R1–R4 molecular junctions

R1	R2	R3	R4
0.28 e	0.29 e	0.31 e	0.30 e

2. Total energies and magnetic moments of the R1–R4 molecular junctions in FM / AFM states

The FM and AFM configurations were initialized by assigning parallel and antiparallel spins to the triphenylmethyl radical centers, respectively. The FM configuration is slightly more stable than the AFM configuration, with $\Delta E = -0.01$ eV, suggesting that the system exhibits nearly degenerate spin configurations. This small energy splitting reflects weak magnetic exchange coupling between the radical centers, suggesting that both spin configurations could coexist or switched by external magnetic or electric fields. The FM states retain significant local magnetic moments, while the AFM states have zero magnetic moment, consistent with antiferromagnetic cancellation.

Table S2. Comparison of magnetic moments and total energies between FM and AFM states for the R1–R4 molecular junctions

Junction	R1	R2	R3	R4
FM Magnetic Moment (μB)	1.79	1.79	1.74	1.61
AFM Magnetic Moment (μB)	0.00	0.00	0.00	0.00
FM Total Energy (eV)	-10501.05	-9693.82	-9716.22	-10293.86
AFM Total Energy (eV)	-10501.06	-9693.83	-9716.23	-10293.87
ΔE = EAFM − EFM (eV)	-0.01	-0.01	-0.01	-0.01

3. Transmission spectra of four molecular junctions in the antiparallel spin configuration, and the transmission spectra of R1 under various biases in the parallel spin configuration.

Fig. S1 presents the spin-resolved electronic transmission spectra of four different molecular junctions under the antiparallel spin configuration. As shown in the figure, none of the four molecular structures exhibit significant spin polarization near the Fermi level, and they share similar transmission features below the Fermi level. However, in the energy range above the E_F, their transmission spectra show noticeable differences. Specifically, the transmission coefficients of R1 and R3 exhibit a pronounced decline within the ranges of 1.1–1.6 eV for R1 and 0.5–1.5 eV for R3, indicating the occurrence of destructive quantum interference (DQI) in these energy intervals. In contrast, the transmission spectrum of R2 shows a gradually decreasing trend, suggesting that constructive quantum interference (CQI) dominates its transport behavior. For R4, the transmission spectra under antiparallel and parallel spin configurations are highly similar, both exhibiting Fano resonance features. This further indicates that variations in substituent groups on the molecular backbone can effectively modulate transmission characteristics and thereby influence electronic transport behavior. Furthermore, to verify whether quantum interference persists under realistic operating conditions, we

calculated the transmission spectra of the R1 molecular junction under biases ranging from −0.2 to 0.2 V (Figure S2). The results show that the characteristic interference patterns remain clearly visible within this bias window, indicating that the quantum interference effect remains effective at practical operating voltages.

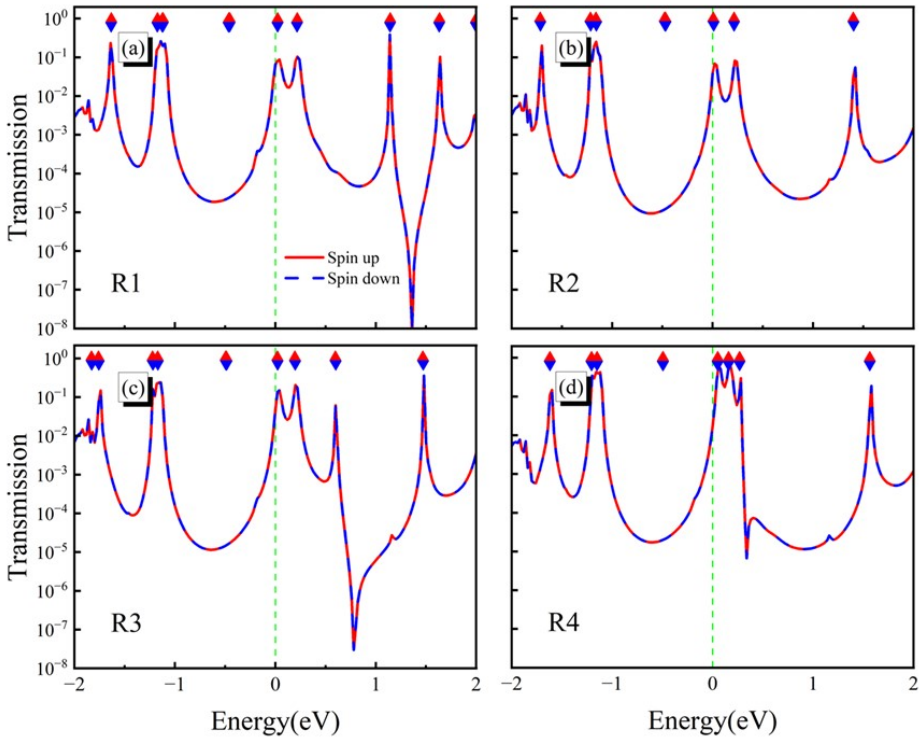

Fig. S1. Spin-resolved electronic transmission spectra as a function of energy for four molecular junctions under antiparallel spin configuration.

4. Spin-resolved transmission pathways of the four molecular junctions

As shown in Fig. S2, the spin-resolved transmission pathways of the R1–R4 systems were calculated at energy positions of 1.36 eV, 1.48 eV, 0.78 eV, and 0.34 eV, respectively, to further reveal their transport mechanisms. It can be observed that the transmission pathways for R1 and R3 are primarily localized within the molecular bridge region. Both spin-up and spin-down channels exhibit weakened pathways or backscattering, indicating strong destructive interference in these regions, which signifies the occurrence of DQI. In contrast, R2 shows uniform and continuous transmission paths, with electrons flowing stably along the molecular backbone without noticeable breaks or local attenuation. This indicates that coherent superposition of electron wavefunctions results in constructive quantum interference (CQI). In comparison, R4 exhibits more complex interference features in its transmission

pathways, which correlate well with the Fano resonance observed in its transmission spectrum (Fig. 2(d)). Although electrons can still propagate through the molecular bridge region in the transmission pathway map, certain localized areas exhibit significant weakening or even disruption of paths, particularly in regions where strong localized discrete states are present, leading to pronounced suppression of electron transport. Moreover, compared with R2, the transmission pathways in R4 are no longer uniformly distributed but show localized attenuation and enhanced dispersion of electron flow, suggesting that coupling between discrete and continuum states gives rise to localized resonant states. This characteristic is consistent with the physical mechanism of Fano resonance, where quantum transitions of discrete states interfere coherently with electron transport in continuum states, resulting in a characteristic peak–dip structure. Therefore, the substituents in R4 not only alter the local electron distribution of the molecular orbitals but also introduce additional scattering pathways, leading to strong interference effects in certain energy regions and the emergence of Fano resonance.

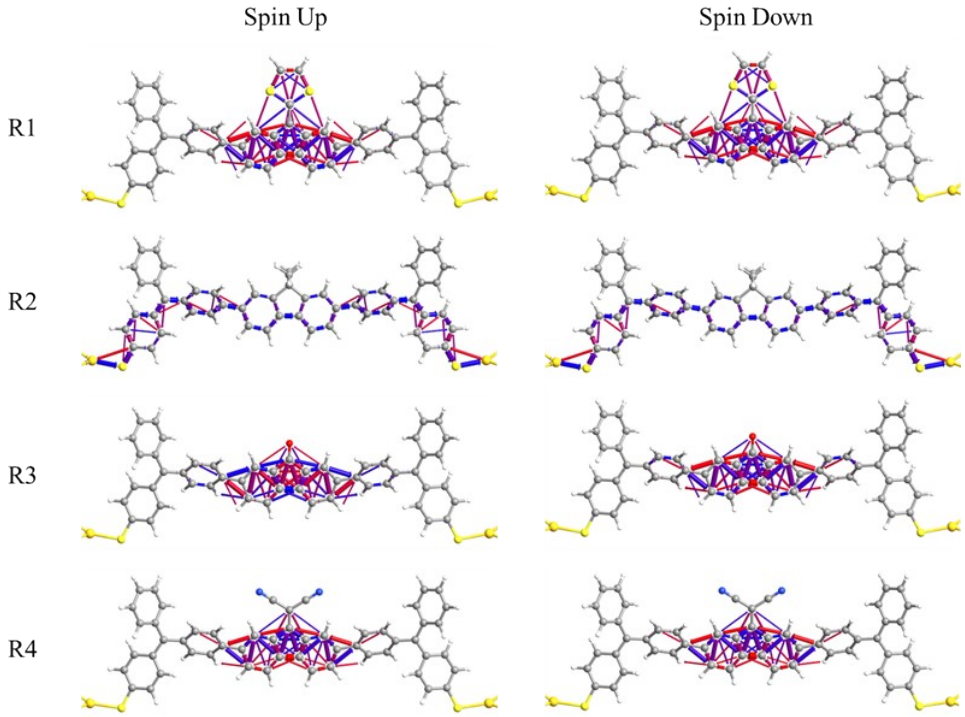

Fig. S2. Spin-resolved transmission pathways of R1–R4 under the parallel spin configuration.

5. Transmission eigenchannels of the four molecular junctions at the E_F.

As shown in Fig. S3, the eigenstates of the spin-up eigenchannels (ECs) for R1–R3 exhibit delocalized distributions across the entire molecular junction, indicating that electrons can be smoothly transmitted through the junctions. In contrast, the eigenstates of the spin-down ECs are localized on the left electrode and the left portion of the molecule, suggesting that electron transport is significantly suppressed in this channel. In comparison, R4 exhibits more balanced transport behavior, with both spin-up and spin-down ECs showing relatively continuous and well-coupled distributions. This implies that the molecular orbitals of R4 are less influenced by spin-selective modulation, which is further corroborated by its transmission spectrum. From the perspective of molecular orbitals, the efficient spin-up conductance observed in R1–R3 mainly originates from the α-HOMO orbitals located near the Fermi level, which exhibit delocalized electron density across the entire molecular framework.

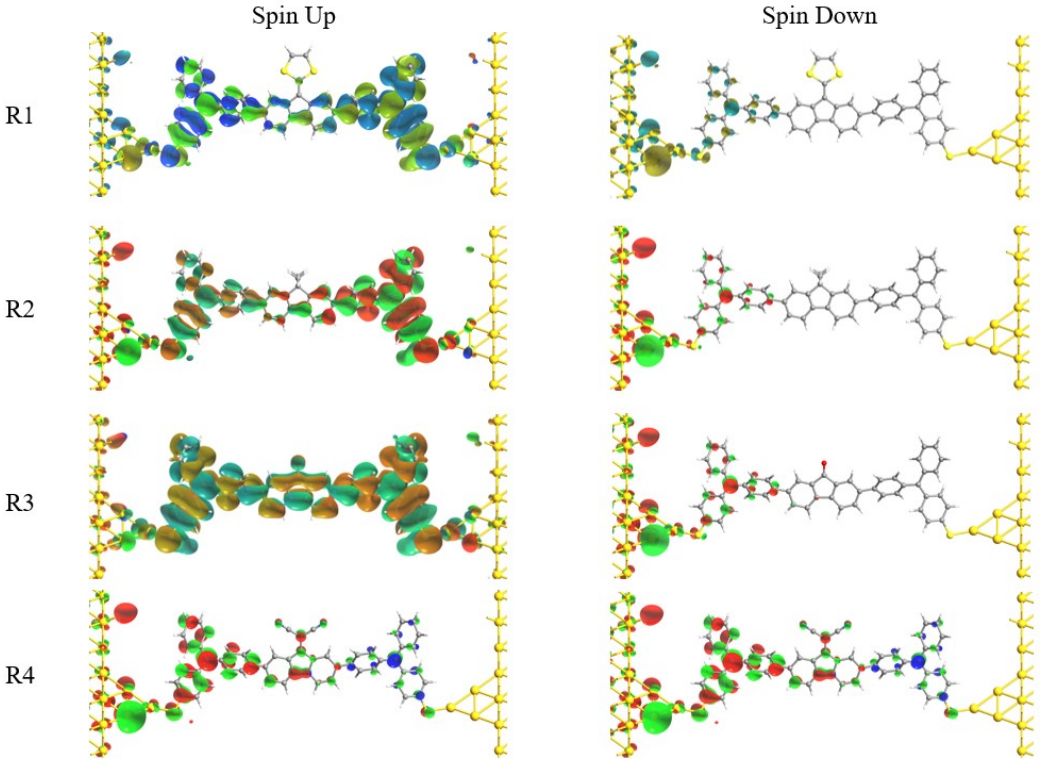

Fig. S3. Spin-up and spin-down transmission eigenchannels of R1–R4 at the E_F

6. Transmission spectra of R1 molecular junction under different biases

Fig. S4 presents the transmission spectra of the R1 molecular junction in the parallel spin configuration under a bias range of −0.2 to 0.2 V. As shown in Fig. S4. (a)–(i), the characteristic quantum interference features remain clearly visible within the

bias window even when a finite voltage is applied, demonstrating that the quantum interference effect is still well preserved under realistic operating conditions. This further confirms the robustness of the interference behavior and highlights its potential applicability in practical device operations.

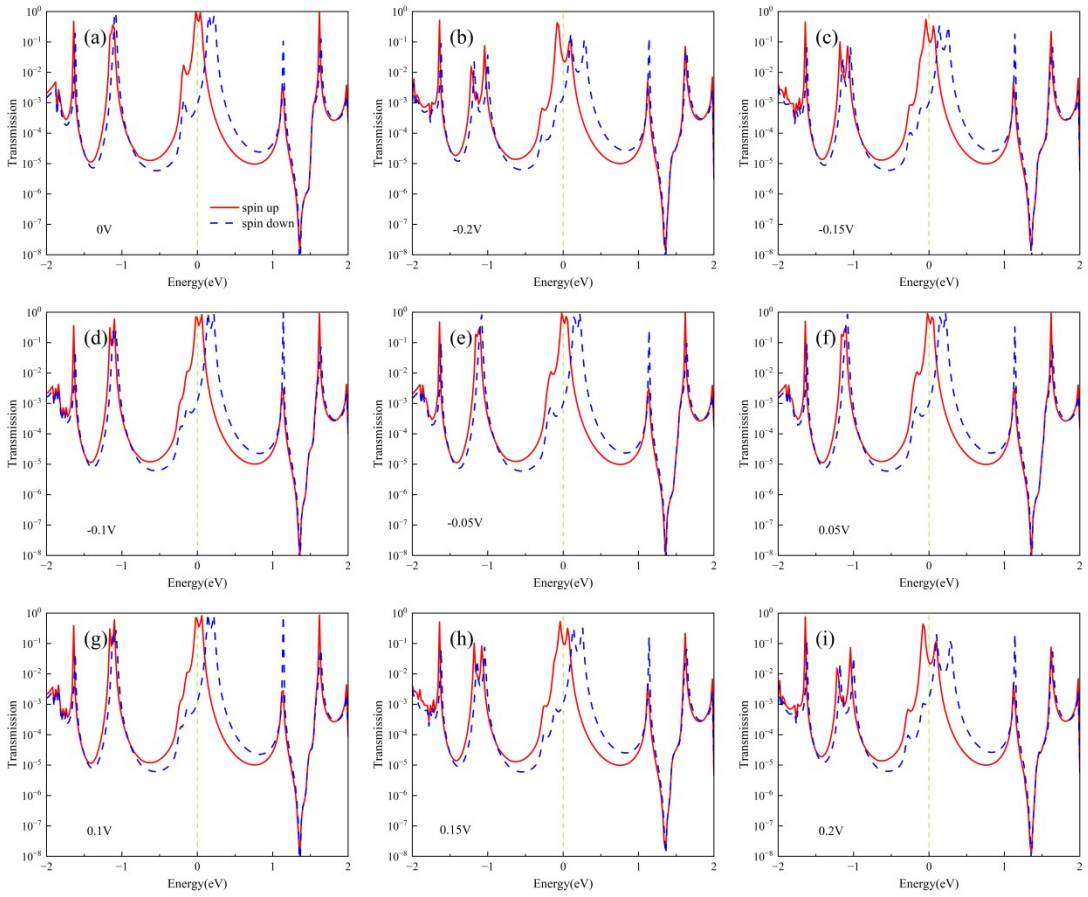

Fig. S4. Transmission spectra of the R1 molecular junction under different biases in the parallel spin configuration.

7. Spin-Resolved Projected Density of States (PDOS) of R1–R3 Molecular Junctions

As shown in Fig. S5, at zero bias (left panel of each figure), the projected density of states (PDOS) for the three molecular junctions are completely degenerate, indicating the absence of magnetic behavior in the system. However, as the bias voltage increases to 0.1 V and 0.2 V, the frontier states near the Fermi level gradually develop slight spin polarization. This phenomenon suggests that the applied bias breaks the spin symmetry of the system, thereby inducing spin-selective electron transport within the molecular junctions. This finding further deepens our understanding of the spin transport mechanism in antiferromagnetic (AFM) systems.

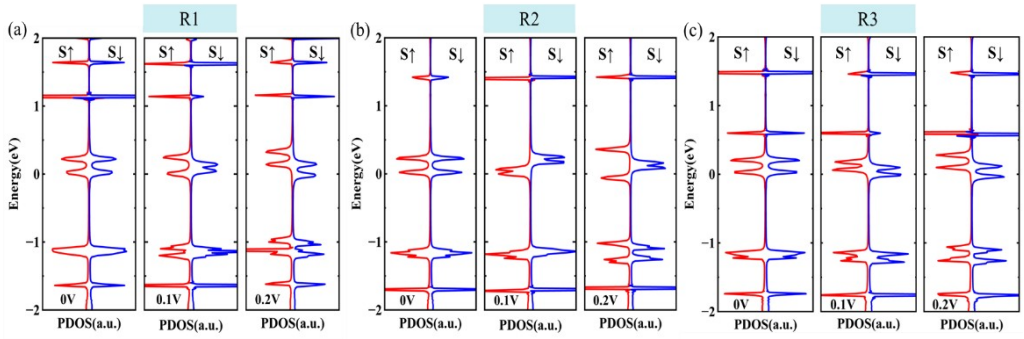

Fig. S5. Spin-resolved projected density of states (PDOS) of R1–R3 (a–c) under the antiferromagnetic configuration at 0 V, 0.1 V, and 0.2 V.

8. Phonon Transmission Spectra of the Four molecular junctions.

Fig. S6 presents the phonon transmission spectra as a function of energy for four different MJs (R1–R4), highlighting the differences in their phonon transport characteristics. As shown, all molecular structures exhibit pronounced transmission peaks in the low-frequency region (0~25 meV), while the phonon transmission function rapidly decays to nearly zero in the high-frequency region above 25 meV, indicating that low-frequency phonons are the dominant carriers for thermal transport. Specifically, R2 shows relatively strong transmission in the mid-to-low frequency range (10~15 meV), suggesting the presence of more phonon channels and a higher phonon thermal conductance. In contrast, R3 displays narrower and weaker transmission peaks, especially in the low-frequency region, indicating reduced phonon transport efficiency consistent with its lower phonon thermal conductance. R1 and R4 exhibit moderate phonon transmission characteristics, with certain frequency ranges showing enhanced transmission, though their overall spectra are more evenly distributed. These results suggest that radical substitution and molecular structural

tuning can significantly influence phonon mode coupling and propagation pathways, thereby modulating the phonon thermal conductance of the junctions and offering a rational design strategy for optimizing thermoelectric performance.

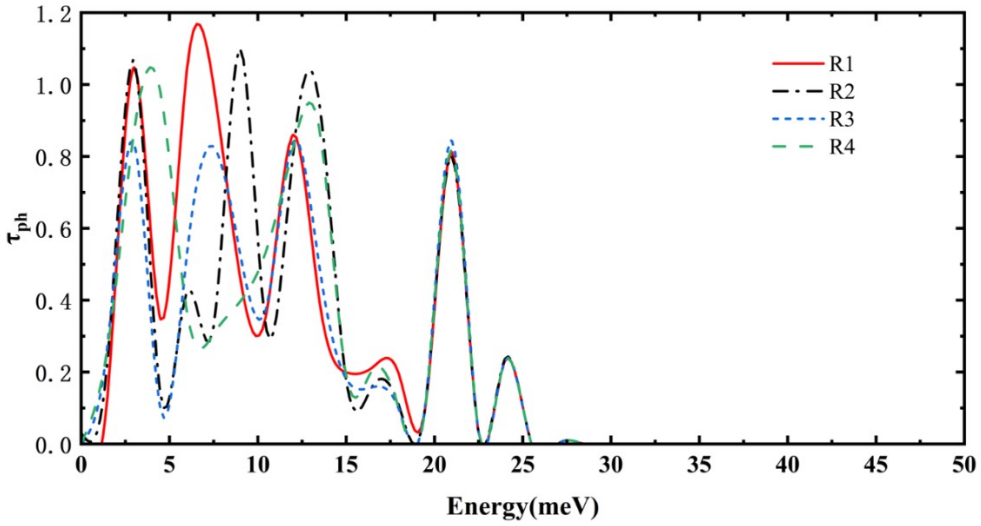

Fig. S6. Phonon transmission spectra of R1–R4 molecular junctions.

9. Temperature dependent thermoelectric properties of the three open-shell molecular junctions

Fig. S7 shows the temperature dependence of the thermoelectric performance of the three open-shell molecular junctions at the Fermi level. As illustrated in Fig. S7(a)–(c), the ZT_{sp} values increase with temperature, reach a maximum, and then decrease at higher temperatures, and the variation in ZT_{sp} is mainly governed by the change in the power factor (*PF*). This trend is consistent with that reported in other studies[1, 2].

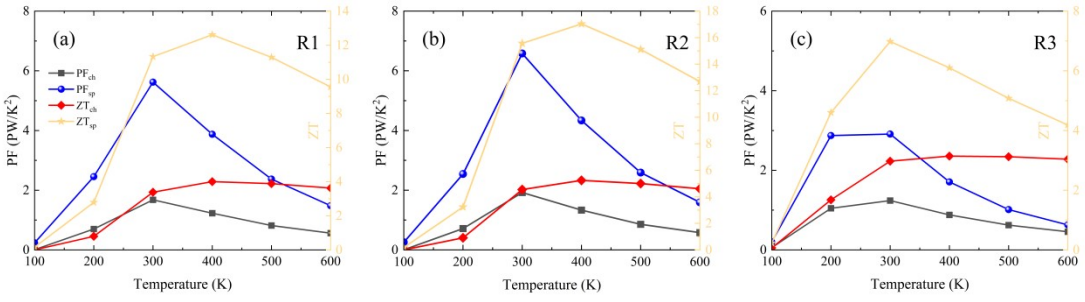

Fig. S7. Temperature dependence of *ZT* and power factor for the R1–R3 molecular junctions at the Fermi level.

References

1. Q. H. Al-Galiby, H. Sadeghi, D. Z. Manrique and C. Lambert, Nanoscale, 2017, 9, 4819-4825.
2. B. Qin, D. Wang, X. Liu, Y. Qin, J.-F. Dong, J. Luo, J.-W. Li, W. Liu, G. Tan and X. Tang, Science, 2021, 373, 556-561.